International Journal of Solids and Structures 48 (2011) 2706–2717

Contents lists available at ScienceDirect

International Journal of Solids and Structures

journal homepage: www.elsevier.com/locate/ijsolstr

New, real fundamental solutions to the transient thermal contact problem in a piezoelectric strip under the coupling actions of a rigid punch and a convective heat supply

Yue Ting Zhou, Kang Yong Lee *

School of Mechanical Engineering, Yonsei University, Seoul 120-749, Republic of Korea

ARTICLE INFO

Article history:
Received 3 January 2011
Received in revised form 6 May 2011
Available online 26 May 2011

Keywords:
Piezoelectric materials
Transient thermal contact
Convective heat supply
Temperature distribution
Stress distribution

ABSTRACT

A thermo-electro-mechanical contact analysis has been performed for a finite piezoelectric strip, which is subjected to the joint actions of a rigid, flat punch and a transient convective heat supply. The Laplace transform and Fourier sine and cosine transforms were applied in solving the governing equations. A detailed analysis of the characteristic roots of the corresponding characteristic equation was made. Real fundamental solutions were derived, which can readily lead to real solutions to the thermo-electro-mechanical quantities. A Cauchy-type singular integral equation was obtained for the stated problem and then solved numerically. Closed form solutions of a special case were obtained. To obtain the accurate solution in the time domain, an effective numerical inversion algorithm of the Laplace transform was applied. Detailed analyses were performed to reveal the variation law of temperature, contact stress beneath the punch, stress intensity factor at the punch edge and strain with time. Parametric studies were performed to discover the effects of the layer thickness on the distribution of temperature, contact stress beneath the punch and stress intensity factor at the punch edge.

1. Introduction

Due to the coupling characteristics between electric and mechanical fields, piezoelectric materials have been widely used in many high-tech areas (Galassi et al., 2000). Piezoelectric materials have proven to be versatile tools for technical measurements and process controls in almost all modern industries.

Contact in piezoelectric materials is of great scientific and technological significance in many areas of study (Giannakopoulos and Suresh, 1999). Much attention has been paid to the contact problems in piezoelectric materials. Using the state space method, Sosa and Castro (1994) obtained solutions for a piezoelectric half-plane loaded by a concentrated line force and a concentrated line charge. Ding et al. (1996) obtained the solution of a piezoelectric half-space subjected to point forces and point charges. Employing Stroh's formalism, Fan et al. (1996) studied the two-dimensional contact problem of a piezoelectric half-plane and obtained the solutions with loads acting on the boundary of an anisotropic piezoelectric half-plane. Solutions in an explicit form for an elastic piezoelectric ceramic half-space indented by a rigid punch with a parabolic cross-section and flat base were obtained by Podilchuk and Tkachenko (1999). The electro-mechanical properties of piezoelectric composites were evaluated theoretically and experimentally by Saigal et al. (1999), Ramamurty et al. (1999) and Sridhar et al. (2000) by applying the indentation technique. Chen (2000) and Ding et al. (2000) conducted contact analysis for a three-dimensional transversely isotropic, piezoelectric half-space. Chen and Yu (2005) analyzed the micro-scale adhesive contact behavior of a piezoelectric half-space. The axisymmetric contact problem of a piezoelectric layer with a circular indenter on its surface was investigated by Wang and Han (2006). The contact behaviors of a piezoelectric layer with a finite thickness indented by either an insulating or a conducting punch were investigated by Wang et al. (2008). The frictionless and frictional contact problems of a non-homogeneous, piezoelectric layered half-plane were considered by Ke et al. (2008, 2010) who applied the superposition principle and the state vector method.

As piezoelectric materials often work in thermal environments, the thermal behavior of piezoelectric materials has attracted considerable attention. Chandrasekharaiah (1988) presented a generalized linear piezo-thermo-elastic formulation. Irschik and Ziegler (1996) generalized Maysel's influence function approach to thermoelasticity for piezoelectric vibration problems. The piezo-thermo-elastic problem concerned with the control of the thermally induced elastic displacement in an isotropic plate bonded to a piezoelectric plate was treated by Choi et al. (1997). Studies of the piezothermoelasticity of laminated piezoelectric structures were conducted by Tauchert et al. (2000). Ashida and Tauchert

* Corresponding author. Tel./fax: +82 2 2123 2813.
E-mail addresses: zhouyueting@yeah.net (Y.T. Zhou), KYL2813@yonsei.ac.kr (K.Y. Lee).

0020-7683/$ - see front matter © 2011 Elsevier Ltd. All rights reserved.
doi:10.1016/j.ijsolstr.2011.05.020

(2001) examined the transient response of a finite circular disk, one face of which was in contact with a heated body. Ootao and Tanigawa (2001) analyzed the control of the transient thermoelastic displacement in a functionally graded rectangular plate, which was bonded to a piezoelectric plate. Applying the finite element method, Wang and Noda (2001) investigated piezo-thermo-elastic problems in non-homogeneous piezoelectric structures. An exact solution to a non-homogeneous piezoelectric cylinder shell subjected to an axisymmetric thermal load was obtained by Wu et al. (2003). Zhong and Shang (2005) performed an exact analysis of a simply supported non-homogeneous piezoelectric plate. Ootao and Tanigawa (2007), Ootao et al. (2008) and Ootao (2009) treated the transient piezo-thermo-elastic response of a non-homogeneous piezoelectric hollow sphere, a hollow cylinder and multiple structures, respectively.

All the aforementioned articles treated piezoelectric materials subjected to either a pure contact load or a purely thermal load. In fact, piezoelectric materials usually work in a highly complex environment and are subjected to multi-type loads. Moreover, the previous studies were mainly conducted for infinite piezoelectric materials, in which the size effect of the thickness of piezoelectric materials was seldom taken into account. To the authors' knowledge, investigations of the transient thermal contact for a finite piezoelectric strip under the joint actions of a rigid flat punch and a non-uniform heat supply have not been previously reported.

In the present study, the real fundamental solution-based approach is applied to investigate the transient thermal contact behavior of a finite piezoelectric strip under the joint actions of a rigid, flat punch and a convective heat supply from the surrounding media. The Laplace transform and Fourier sine and cosine transforms are employed in solving the transient heat conduction equation and piezoelectric governing equation. A detailed analysis of the eigenvalue distributions of the characteristic equation related to the piezoelectric governing equation is conducted. Real fundamental solutions that can lead to real solutions to the thermo-electro-mechanical quantities are derived for the piezoelectric contact problem. A Cauchy-type singular integral equation is obtained for the stated problem. In particular, closed form solutions of a special case are obtained, which can be used to validate the present numerical computation. An effective numerical inversion algorithm of the Laplace transform is implemented to obtain the solution in the time domain. Parametric studies are performed to discover the effects of the dimensionless time and the layer thickness on the distributions of temperature, contact stress beneath the punch and stress intensity factor at the punch edge.

The present study is innovative in two aspects. On the one hand, the model of the transient thermal contact of a finite piezoelectric strip under the coupling actions of a rigid flat punch and a convective heat supply is of more practical significance than the widely studied model of infinite piezoelectric materials subjected to a purely unitary load. On the other hand, the real fundamental solution-based approach is more straightforward than the traditional complex fundamental solution-based method.

2. Problem statement and formulation

The configuration of the contact problem under consideration is depicted in Fig. 1, in which a rigid, insulated flat punch is indented into the upper surface of a piezoelectric strip with a thickness h under an indentation force P. The lower surface of the layer is bonded to a rigid base. The strip is initially at a uniform temperature zero, and its surface $x = -h$ is suddenly heated from the surrounding base with a temperature $T_0(t)f_0(x)$ and relative surface heat transfer coefficient H_a. Piezoelectric materials are poled along the thickness direction (y-axis).

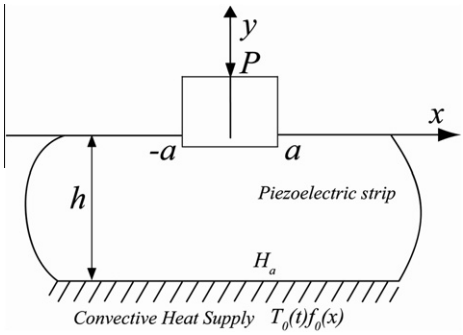

Fig. 1. Piezoelectric strip under the coupling actions of a rigid punch and a transient convection heat supply.

On the one hand, piezoelectric materials are subjected to a non-uniform time-varying heat supply and uniform electric-mechanical loads. On the other hand, the present study is under small deformation conditions. Thus, the problem is routinely handed as uncoupled and quasi-static, i.e., the heat conduction equation and the equations of electric-mechanical are solved in turn, and the inertial effects are negligible.

The transient heat conduction equation takes the following form:

$$k_1\frac{\partial^2 T}{\partial x^2}+k_3\frac{\partial^2 T}{\partial y^2}=\rho c_v\frac{\partial T}{\partial t}, \tag{1}$$

where $T(x,y,t)$ represents the temperature, k_1 and k_3 are the thermal conductivities for the piezoelectric ceramic, ρ and c_v are the mass density and specific heat, respectively, and t is the time variable.

The governing equations for the piezoelectric materials are given as follows:

$$\begin{aligned}
&c_{11}\frac{\partial^2 u}{\partial x^2}+c_{44}\frac{\partial^2 u}{\partial y^2}+(c_{13}+c_{44})\frac{\partial^2 v}{\partial x\partial y}+(e_{31}+e_{15})\frac{\partial^2 \phi}{\partial x\partial y}=\lambda_{11}\frac{\partial T}{\partial x},\\
&(c_{13}+c_{44})\frac{\partial^2 u}{\partial x\partial y}+c_{44}\frac{\partial^2 v}{\partial x^2}+c_{33}\frac{\partial^2 v}{\partial y^2}+e_{15}\frac{\partial^2 \phi}{\partial x^2}+e_{33}\frac{\partial^2 \phi}{\partial y^2}=\lambda_{33}\frac{\partial T}{\partial y},\\
&(e_{15}+e_{31})\frac{\partial^2 u}{\partial x\partial y}+e_{15}\frac{\partial^2 v}{\partial x^2}+e_{33}\frac{\partial^2 v}{\partial y^2}-\in_{11}\frac{\partial^2 \phi}{\partial x^2}-\in_{33}\frac{\partial^2 \phi}{\partial y^2}=-\beta_3\frac{\partial T}{\partial y}.
\end{aligned} \tag{2}$$

The stress and electric displacement can be evaluated from the following constitutive relations:

$$\begin{aligned}
\sigma_{xx}&=c_{11}\frac{\partial u}{\partial x}+c_{13}\frac{\partial v}{\partial y}-e_{31}E_y-\lambda_{11}T,\\
\sigma_{yy}&=c_{13}\frac{\partial u}{\partial x}+c_{33}\frac{\partial v}{\partial y}-e_{33}E_y-\lambda_{33}T,\\
\sigma_{xy}&=c_{44}\left[\frac{\partial u}{\partial y}+\frac{\partial v}{\partial x}\right]-e_{15}E_x,
\end{aligned} \tag{3}$$

$$\begin{aligned}
D_x&=e_{15}\left[\frac{\partial u}{\partial y}+\frac{\partial v}{\partial x}\right]+\in_{11}E_x,\\
D_y&=e_{31}\frac{\partial u}{\partial x}+e_{33}\frac{\partial v}{\partial y}+\in_{33}E_y+\beta_3 T,
\end{aligned} \tag{4}$$

where $u(x,y,t)$ and $v(x,y,t)$ are the displacement components along the x-axis and y-axis, respectively, $\varphi(x,y,t)$ is the electric potential, σ_{xx}, σ_{yy} and σ_{xy} are the stress components, D_x and D_y are the electric displacement components, c_{ij}, e_{ij} and ϵ_{ii} stand for the elastic coefficients, piezoelectric coefficients and dielectric coefficients, respectively, and λ_{ii} and β_3 are the thermal stress coefficients and pyroelectric coefficient. The electric fields E_x and E_y are given as follows:

$$E_x = -\frac{\partial \phi}{\partial x}, \quad E_y = -\frac{\partial \phi}{\partial y}. \tag{5}$$

2.1. Thermal initial and boundary conditions

The initial boundary condition is

$$T = 0, \quad t = 0. \tag{6}$$

The punch is assumed to be insulated. Piezoelectric materials are impervious to heat inside and outside of the contact region on the upper surface, thus

$$k_3 \frac{\partial T(x,0,t)}{\partial y} = 0, \quad |x| < +\infty. \tag{7}$$

On the lower surface $y = -h$, piezoelectric materials receive a convective heat supply from the surrounding base

$$k_3 \frac{\partial T(x,-h,t)}{\partial y} = H_a[T(x,-h,t) - T_0(t)f_0(x)], \quad |x| < +\infty, \tag{8}$$

where $T_0(t)f_0(x)$ is the surrounding temperature and H_a is the relative surface heat transfer coefficient. We assume that $T_0(t)f_0(x)$ is an even function with respect to x and can be Fourier- and Laplace-transformed.

2.2. Electrical boundary conditions

The normal component of the electrical displacement vector should be zero on the upper surface $y = 0$ because the punch is electrical insulated, i.e.,

$$D_y(x,0,t) = 0, \quad |x| < +\infty. \tag{9}$$

On the surface $y = -h$, the piezoelectric ceramic layer is grounded

$$\phi(x,-h,t) = 0, \quad |x| < +\infty. \tag{10}$$

2.3. Mechanical boundary conditions

The normal traction under the punch is unknown and the frictionless condition is modeled. The total normal force along the y-axis inside the contact area equals the indentation force P. Outside the contact area, the stresses are free. Thus,

$$\frac{\partial v(x,0,t)}{\partial x} = 0, \quad |x| < a, \tag{11}$$

$$\sigma_{yy}(x,0,t) = -p(x,t), \quad |x| < a, \tag{12}$$

$$\int_{-a}^{a} \sigma_{yy}(x,0,t)dx = -P, \quad |x| < a, \tag{13}$$

$$\sigma_{yy}(x,0,t) = 0, \quad |x| > a, \tag{14}$$

$$\sigma_{xy}(x,0,t) = 0, \quad |x| < +\infty, \tag{15}$$

where $p(x,t)$ is the unknown contact pressure under the punch.

On the surface $y = -h$, it is modeled that the layer dose not bend, i.e.,

$$u(x,-h,t) = 0, \quad |x| < +\infty, \tag{16}$$

$$v(x,-h,t) = 0, \quad |x| < +\infty. \tag{17}$$

3. Temperature field

The Laplace transform pairs are given as follows:

$$w^*(\xi) = \int_0^\infty w(t)e^{-\xi t}dt, \quad w(t) = \frac{1}{2\pi i}\int_{Br} w^*(\xi)e^{\xi t}d\xi, \tag{18}$$

where Br indicates the Bromwich path of integration.

By applying the Laplace transform to Eq. (1), one has

$$k_{10}\frac{\partial^2 T^*}{\partial x^2} + \frac{\partial^2 T^*}{\partial y^2} = \frac{\xi}{D_3}T^*, \tag{19}$$

where $T^*(x,y,p)$ is the Laplace transform of $T(x,y,t)$, $D_3 = k_3/\rho \cdot c$ is the principal thermal diffusivity along the principal y-axis, and

$$k_{10} = \frac{k_1}{k_3}. \tag{20}$$

The thermal boundary conditions in the Laplace-transformed plane are as follows:

$$k_3 \frac{\partial T^*(x,0,\xi)}{\partial y} = 0, \tag{21}$$

$$k_3 \frac{\partial T^*(x,-h,\xi)}{\partial y} = H_a[T^*(x,-h,\xi) - T_0^*(\xi)f_0(x)], \tag{22}$$

where $T_0^*(\xi)$ is the Laplace transform of $T_0(t)$.

By applying the Fourier transform with respect to x, one obtains the following general solution of Eq. (19):

$$T^* = \frac{2}{\pi}\int_0^\infty (A_1 e^{n_1 y} + A_2 e^{n_2 y})\cos(\omega x)d\omega, \tag{23}$$

where ω is the Fourier transform variable, $A_j (j = 1,2)$ are unknown functions to be determined from the thermal boundary conditions, and $n_j (j = 1,2)$ are related to the following characteristic equation and are given by:

$$n^2 - \left(k_{10}\omega^2 + \frac{\xi}{D_3}\right) = 0, \quad n_{1,2} = \pm\sqrt{k_{10}\omega^2 + \frac{\xi}{D_3}}. \tag{24}$$

Considering boundary conditions (21) and (22) in the ξ-plane, one obtains A_j $(j = 1,2)$ as follows:

$$\begin{aligned} A_1 &= \frac{\pi}{2}\frac{-n_2 H_a T_0^*(\xi)f(\omega)}{n_2(k_3 n_1 - H_a)e^{n_2 h} - n_1(k_3 n_2 - H_a)e^{n_1 h}}, \\ A_2 &= \frac{\pi}{2}\frac{n_1 H_a T_0^*(\xi)f(\omega)}{n_2(k_3 n_1 - H_a)e^{n_2 h} - n_1(k_3 n_2 - H_a)e^{n_1 h}}, \end{aligned} \tag{25}$$

where

$$f(\omega) = \int_0^\infty f_0(x)\cos(\omega x)dx. \tag{26}$$

4. Mechanical and electric displacement field

Employing the Laplace transform to Eq. (2) produces:

$$\begin{aligned} &c_{11}\frac{\partial^2 u^*}{\partial x^2} + c_{44}\frac{\partial^2 u^*}{\partial y^2} + (c_{13}+c_{44})\frac{\partial^2 v^*}{\partial x \partial y} + (e_{31}+e_{15})\frac{\partial^2 \phi^*}{\partial x \partial y} = \lambda_{11}\frac{\partial T^*}{\partial x}, \\ &(c_{13}+c_{44})\frac{\partial^2 u^*}{\partial x \partial y} + c_{44}\frac{\partial^2 v^*}{\partial x^2} + c_{33}\frac{\partial^2 v^*}{\partial y^2} + e_{15}\frac{\partial^2 \phi^*}{\partial x^2} + e_{33}\frac{\partial^2 \phi^*}{\partial y^2} = \lambda_{33}\frac{\partial T^*}{\partial y}, \\ &(e_{15}+e_{31})\frac{\partial^2 u^*}{\partial x \partial y} + e_{15}\frac{\partial^2 v^*}{\partial x^2} + e_{33}\frac{\partial^2 v^*}{\partial y^2} - \in_{11}\frac{\partial^2 \phi^*}{\partial x^2} - \in_{33}\frac{\partial^2 \phi^*}{\partial y^2} = -\beta_3\frac{\partial T^*}{\partial y} \end{aligned} \tag{27}$$

The electrical and mechanical boundary conditions in the ξ-plane are as follows:

$$D_y^*(x,0,\xi) = 0, \quad |x| < +\infty, \tag{28}$$

$$\phi^*(x,-h,\xi) = 0, \quad |x| < +\infty, \tag{29}$$

$$\frac{\partial v^*(x,0,\xi)}{\partial x} = 0, \quad |x| < a, \tag{30}$$

$$\sigma_{yy}^*(x,0,\xi) = -p^*(x,\xi), \quad |x| < a, \tag{31}$$

$$\int_{-a}^{a} \sigma_{yy}^*(x,0,\xi)dx = -\frac{P}{\xi}, \quad |x| < a, \tag{32}$$

$$\sigma^*_{yy}(x,0,\xi)=0, \quad |x|>a, \tag{33}$$
$$\sigma^*_{xy}(x,0,\xi)=0, \quad |x|<+\infty, \tag{34}$$
$$u^*(x,-h,\xi)=0, \quad |x|<+\infty, \tag{35}$$
$$v^*(x,-h,\xi)=0, \quad |x|<+\infty, \tag{36}$$

where $D^*_y, \phi^*, \sigma^*_{ij}, u^*$ and v^* are the Laplace transforms of D_y, ϕ, σ_{ij}, u and v, respectively.

The mechanical displacements and electric potential are obtained as follows:

$$u^*(x,y,\xi)=\frac{2}{\pi}\int_0^\infty U_{c\omega}(y)\sin(\omega x)d\omega+\frac{2}{\pi}\int_0^\infty\sum_{k=1}^{2}\frac{F_{1k}}{\omega}\sin(\omega x)A_k e^{n_k y}d\omega,$$
$$v^*(x,y,\xi)=\frac{2}{\pi}\int_0^\infty V_{c\omega}(y)\cos(\omega x)d\omega+\frac{2}{\pi}\int_0^\infty\sum_{k=1}^{2}\frac{F_{2k}}{\omega}\cos(\omega x)A_k e^{n_k y}d\omega, \tag{37}$$

$$\phi^*(x,y,\xi)=\frac{2}{\pi}\int_0^\infty \Phi_{c\omega}(y)\cos(\omega x)d\omega+\frac{2}{\pi}\int_0^\infty\sum_{k=1}^{2}\frac{F_{3k}}{\omega}\times\cos(\omega x)A_k e^{n_k y}d\omega, \tag{38}$$

where the first term on the right-hand sides gives the homogeneous solution and the second term on the right-hand sides gives the particular solution arising from the temperature field. In the following, these solutions will be given, respectively.

We now consider the homogeneous solutions. The quantities $[U_{c\omega}(y)\ V_{c\omega}(y)\ \Phi_{c\omega}(y)]$ may be expressed as:

$$[U_{c\omega}(y)\ V_{c\omega}(y)\ \Phi_{c\omega}(y)]^T=\left[U^0_{c\omega}(y)\ V^0_{c\omega}(y)\ \Phi^0_{c\omega}(y)\right]^T e^{\omega\eta y}. \tag{39}$$

Substituting Eq. (39) into Eq. (27) yields the following characteristic equation:

$$\begin{bmatrix} c_{11}-c_{44}(\eta_j)^2 & (c_{13}+c_{44})\eta_j & (e_{31}+e_{15})\eta_j \\ (c_{13}+c_{44})\eta_j & c_{33}(\eta_j)^2-c_{44} & e_{33}(\eta_j)^2-e_{15} \\ (e_{31}+e_{15})\eta_j & e_{33}(\eta_j)^2-e_{15} & \in_{11}-\in_{33}(\eta_j)^2 \end{bmatrix}\begin{bmatrix} U^0_{c\omega} \\ V^0_{c\omega} \\ \Phi^0_{c\omega}\end{bmatrix}=0. \tag{40}$$

Eq. (40) is a sextic equation. There are six roots for η_j. The roots are of the forms: (1) the complex roots appear in conjugate pairs; (2) the opposite roots η_n and $-\eta_n$ $(n=1,2,3)$ appear in pairs. In the view of mathematics, the eigenvalues are of the following cases:

(i) three pairs of opposite real roots;
(ii) two pairs of opposite real roots and a pair of purely imaginary roots;
(iii) a pair of opposite real roots and two pairs of purely imaginary roots;
(iv) a pair of opposite real roots and two pairs of complex conjugate roots (no purely imaginary roots);
(v) three pairs of complex conjugate roots including only one pair of purely imaginary roots;
(vi) three pairs of purely imaginary roots.

Generally speaking, for the commercially available piezoelectric materials, the eigenvalues are distinct, i.e., $\eta_1\neq\eta_2\neq\eta_3$. Furthermore, there are three eigenvalues whose real parts are positive, while the others have negative real parts. Thus, case (i) and (iv) will occur in the practical computation. For convenience in further derivations, we rearrange case (i) as case A, and case (iv) as case B.

Thus, $[U_{c\omega}(y)\ V_{c\omega}(y)\ \Phi_{c\omega}(y)]^T$ can be obtained in terms of real fundamental solutions $\Theta_j=[\Theta_{1j}(\omega,y)\ \Theta_{2j}(\omega,y)\ \Theta_{3j}(\omega,y)]^T$ $(j=1,\ldots,6)$ as follows:

$$[U_{c\omega}(y)\ V_{c\omega}(y)\ \Phi_{c\omega}(y)]^T=\sum_{j=1}^{6}M_j[\Theta_{1j}(\omega,y)\ \Theta_{2j}(\omega,y)\ \Theta_{3j}(\omega,y)]^T, \tag{41}$$

where M_j $(j=1,\ldots,6)$ are the unknown functions to be determined from the boundary conditions.

For Case A, there are three pairs of opposite real roots

$$\eta_1=-\eta_4, \quad \eta_2=-\eta_5, \quad \eta_3=-\eta_6, \tag{42}$$

where $\eta_n>0$ $(n=1,2,3)$. The real fundamental solutions $\Theta j=[\Theta_{1j}(\omega,y)\ \Theta_{2j}(\omega,y)\ \Theta_{3j}(\omega,y)]^T$ $(j=1,\ldots,6)$ are given as:

$$\Theta_1=e^{\omega\eta_1 y}\begin{bmatrix}1\\ f(\eta_1)\\ g(\eta_1)\end{bmatrix}, \quad \Theta_2=e^{\omega\eta_2 y}\begin{bmatrix}1\\ f(\eta_2)\\ g(\eta_2)\end{bmatrix}, \quad \Theta_3=e^{\omega\eta_3 y}\begin{bmatrix}1\\ f(\eta_3)\\ g(\eta_3)\end{bmatrix},$$
$$\Theta_4=e^{-\omega\eta_1 y}\begin{bmatrix}-1\\ f(\eta_1)\\ g(\eta_1)\end{bmatrix}, \quad \Theta_5=e^{-\omega\eta_2 y}\begin{bmatrix}-1\\ f(\eta_2)\\ g(\eta_2)\end{bmatrix}, \quad \Theta_6=e^{-\omega\eta_3 y}\begin{bmatrix}-1\\ f(\eta_3)\\ g(\eta_3)\end{bmatrix}, \tag{43}$$

where the functions $f()$, $g()$ are defined as:

$$f(\eta_j)=\frac{(e_{31}+e_{15})(c_{13}+c_{44})(\eta_j)^2-[c_{11}-c_{44}(\eta_j)^2][e_{33}(\eta_j)^2-e_{15}]}{(c_{13}+c_{44})\eta_j[e_{33}(\eta_j)^2-e_{15}]-(e_{31}+e_{15})\eta_j[c_{33}(\eta_j)^2-c_{44}]},$$
$$g(\eta_j)=\frac{[c_{11}-c_{44}(\eta_j)^2][c_{33}(\eta_j)^2-c_{44}]-(c_{13}+c_{44})^2(\eta_j)^2}{(c_{13}+c_{44})\eta_j[e_{33}(\eta_j)^2-e_{15}]-(e_{31}+e_{15})\eta_j[c_{33}(\eta_j)^2-c_{44}]}. \tag{44}$$

For Case B, there are a pair of opposite real roots and two pairs of complex conjugate roots

$$\eta_1=-\eta_4=\tau_0, \quad \eta_2=-\eta_5=\mu+iv, \quad \eta_3=-\eta_6=\mu-iv, \tag{45}$$

where $i^2=-1$, $\tau_0>0$, $\mu>0$ and $v>0$. The real fundamental solutions $\Theta_j=[\Theta_{1j}(\omega,y)\ \Theta_{2j}(\omega,y)\ \Theta_{3j}(\omega,y)]^T$ $(j=1,\ldots,6)$ are given as:

$$\Theta_1=e^{\omega\tau_0 y}\begin{bmatrix}1\\ f(\tau_0)\\ g(\tau_0)\end{bmatrix}, \quad \Theta_4=e^{-\omega\tau_0 y}\begin{bmatrix}-1\\ f(\tau_0)\\ g(\tau_0)\end{bmatrix},$$
$$\Theta_2=e^{\omega\mu y}\begin{bmatrix}\cos(\omega v Y)\\ \Gamma_1\cos(\omega v y)-\Delta_1\sin(\omega v y)\\ \Gamma_2\cos(\omega v y)-\Delta_2\sin(\omega v y)\end{bmatrix},$$
$$\Theta_3=e^{\omega\mu y}\begin{bmatrix}\sin(\omega v y)\\ \Delta_1\cos(\omega v y)+\Gamma_1\sin(\omega v y)\\ \Delta_2\cos(\omega v y)+\Gamma_2\sin(\omega v y)\end{bmatrix}, \tag{46}$$
$$\Theta_5=e^{-\omega\mu y}\begin{bmatrix}\cos(\omega v y)\\ -\Gamma_1\cos(\omega v y)-\Delta_1\sin(\omega v y)\\ -\Gamma_2\cos(\omega v y)-\Delta_2\sin(\omega v y)\end{bmatrix},$$
$$\Theta_6=e^{-\omega\mu y}\begin{bmatrix}-\sin(\omega v y)\\ -\Delta_1\cos(\omega v y)+\Gamma_1\sin(\omega v y)\\ -\Delta_2\cos(\omega v y)+\Gamma_2\sin(\omega v y)\end{bmatrix},$$

where

$$\Gamma_1=Re[f(\eta_2)], \quad \Delta_1=Im[f(\eta_2)],$$
$$\Gamma_2=Re[g(\eta_2)], \quad \Delta_2=Im[g(\eta_2)], \quad \eta_2=\mu+iv. \tag{47}$$

In Eq. (47), $Re[]$ and $Im[]$ stand for the real part and imaginary part, respectively. The functions $f()$ and $g()$ appearing in Eqs. (46) and (47) are defined in Eq. (44).

It is worth noting that Eqs. (43) and (46) give the real fundamental solutions rather than the classical complex fundamental

solutions, which possess the same form as Eq. (43). Thus, it is straightforward to conduct the subsequent analysis.

As mentioned above, the second term on the right-hand sides of Eqs. (37) and (38) gives the particular solutions arising from the temperature field. The known functions $F_{mk}(\omega)$ ($m = 1,2,3$, $k = 1,2$) appearing in Eqs. (37) and (38) are given as follows:

$$F_{mk} = (-1)^m \left[-\lambda_{11} \frac{H^{(k)}_{1,m}}{H^{(k)}} + \lambda_{33} n_k \frac{H^{(k)}_{2,m}}{H^{(k)}} + \beta_3 n_k \frac{H^{(k)}_{3,m}}{H^{(k)}} \right], \tag{48}$$

where $H^{(k)}$ ($k = 1,2$) are the determinants of the coefficient matrices of systems of linear algebraic equations and $H^{(k)}_{i,j}$ ($k = 1,2$, $i,j = 1,2,3$) are the subdeterminants of the same matrix corresponding to the elimination of the ith row and jth column. The systems of linear algebraic equations are given as:

$$A^{(k)}_H \times X^{(k)}_H = B^{(k)}_H, \quad k = 1,2, \tag{49}$$

where $A^{(k)}_H = \left[a^{(k)}_{ij}\right]$, $a^{(k)}_{ij}$ ($k = 1,2$, $i,j = 1,2,3$) are given in Appendix A, X_H and B_H are given as:

$$X^{(k)}_H = [F_{1k}\ F_{2k}\ F_{3k}]^T, \quad B^{(k)}_H = [\lambda_{11}\ \lambda_{33} n_k\ -\beta_3 n_k]^T, \tag{50}$$

where the superscript "T" represents the transposition of a vector.

Inserting Eqs. (23), (37), (39), (41), (43) and (46) into Eqs. (3) and (4) in the Laplace-transformed plane, one obtains the following expressions of stresses and electric displacement:

$$\begin{aligned}
\sigma^*_{xx} &= \frac{2}{\pi} \int_0^\infty \sum_{j=1}^{6} \omega \Omega_{0j}(\omega, y) M_j(\omega) \cos(\omega x) d\omega \\
&\quad + \frac{2}{\pi} \int_0^\infty \sum_{k=1}^{2} \mathrm{T}_{0k} \cos(\omega x) A_k e^{n_k y} d\omega, \\
\sigma^*_{yy} &= \frac{2}{\pi} \int_0^\infty \sum_{j=1}^{6} \omega \Omega_{1j}(\omega, y) M_j(\omega) \cos(\omega x) d\omega \\
&\quad + \frac{2}{\pi} \int_0^\infty \sum_{k=1}^{2} \mathrm{T}_{1k} \cos(\omega x) A_k e^{n_k y} d\omega, \\
\sigma^*_{xy} &= \frac{2}{\pi} \int_0^\infty \sum_{j=1}^{6} \omega \Omega_{2j}(\omega, y) M_j(\omega) \sin(\omega x) d\omega \\
&\quad + \frac{2}{\pi} \int_0^\infty \sum_{k=1}^{2} \mathrm{T}_{2k} \sin(\omega x) A_k e^{n_k y} d\omega, \\
D^*_y &= \frac{2}{\pi} \int_0^\infty \sum_{j=1}^{6} \omega \Omega_{3j}(\omega, y) M_j(\omega) \cos(\omega x) d\omega \\
&\quad + \frac{2}{\pi} \int_0^\infty \sum_{k=1}^{2} \mathrm{T}_{3k} \cos(\omega x) A_k e^{n_k y} d\omega,
\end{aligned} \tag{51, 52}$$

where $\Omega_{nj}(\omega, y)$ ($n = 0,1,2,3$, $j = 1,\ldots,6$) and $\mathrm{T}_{nk}(\omega)$ ($n = 0,1,2,3$, $k = 1,2$) are given in Appendix A.

After considering the mechanical boundary conditions (28), (29), (33)–(36) and applying the Fourier sine and cosine transforms accordingly, the unknown functions M_j ($j = 1,\ldots,6$) can be expressed as the following form:

$$M_j = \frac{1}{\omega} \sum_{m=1}^{6} (-1)^{m+j} \frac{H_{mj}}{H} G_m + \frac{(-1)^{1+j} F}{\omega} \frac{H_{1j}}{H}, \tag{53}$$

where H is the determinant of matrix $A_H = [a_{ij}]$ ($i,j = 1,\ldots,6$) and H_{ij} ($i,j = 1,\ldots,6$) are the subdeterminants of the same matrix corresponding to the elimination of the ith row and jth column. The matrix $[a_{ij}]$ ($i,j = 1,\ldots,6$), G_j ($j = 1,\ldots,6$) and F are given as follows:

$$\begin{aligned}
&a_{1j} = \Omega_{1j}(\omega, 0), \quad a_{2j} = \Omega_{2j}(\omega, 0), \quad a_{3j} = \Omega_{3j}(\omega, 0), \\
&a_{4j} = \Theta_{1j}(\omega, -h), \quad a_{5j} = \Theta_{2j}(\omega, -h), \quad a_{6j} = \Theta_{3j}(\omega, -h),
\end{aligned} \tag{54}$$

$$\begin{aligned}
&G_1 = -\sum_{k=1}^{2} \mathrm{T}_{1k} A_k, \quad G_2 = -\sum_{k=1}^{2} \mathrm{T}_{2k} A_k, \quad G_3 = -\sum_{k=1}^{2} \mathrm{T}_{3k} A_k, \\
&G_4 = -\sum_{k=1}^{2} F_{1k} A_k e^{-n_k h}, \quad G_5 = -\sum_{k=1}^{2} F_{2k} A_k e^{-n_k h}, \quad G_6 = -\sum_{k=1}^{2} F_{3k} A_k e^{-n_k h},
\end{aligned} \tag{55}$$

$$F(\omega, \xi) = \int_0^a \sigma_{yy}(s, 0, \xi) \cos(\omega s) ds. \tag{56}$$

5. Integral equations

Considering Eqs. (23), (37), (39) and (41), one obtains:

$$\frac{\partial v^*(x, 0, \xi)}{\partial x} = -\frac{1}{\pi} \int_{-a}^{a} N_1(x, s) \sigma^*_{yy}(s, 0, \xi) ds - \frac{2}{\pi} N_2(x), \tag{57}$$

where the kernels N_j ($j = 1,2$) are given as:

$$\begin{aligned}
N_1(x, s) &= \int_0^\infty L_1(\omega) \cos(\omega s) \sin(\omega x) d\omega, \\
N_2(x) &= \int_0^\infty L_2(\omega) \sin(\omega x) d\omega,
\end{aligned} \tag{58}$$

where

$$\begin{aligned}
L_1(\omega) &= \sum_{j=1}^{6} (-1)^{1+j} \Theta_{2j}(\omega, 0) \frac{H_{1j}}{H}, \\
L_2(\omega) &= \sum_{j=1}^{6} \sum_{m=1}^{6} (-1)^{m+j} \Theta_{2j}(\omega, 0) \frac{H_{mj}}{H} G_m + \sum_{k=1}^{2} F_{2k} A_k.
\end{aligned} \tag{59}$$

As ω approaches infinity, the following asymptotic value of $L_1(\omega)$ can be obtained:

$$\lim_{\omega \to \infty} L_1(\omega) = \Lambda_1 \quad (i = 1,2). \tag{60}$$

After taking into account the following formulas:

$$\int_0^\infty \cos(\omega s) \sin(\omega x) d\omega = \frac{1}{2} \left(\frac{1}{s + x} - \frac{1}{s - x} \right) \tag{61}$$

separating the leading terms in Eq. (60) and considering the odd–even properties of $\sigma_{yy}(x, 0, \xi)$, Eq. (57) can be rewritten as follows:

$$\begin{aligned}
\frac{\partial v^*(x, 0, \xi)}{\partial x} &= -\frac{1}{\pi} \int_{-a}^{a} \frac{\Lambda_1}{s - x} \sigma^*_{yy}(s, 0, \xi) ds \\
&\quad - \frac{1}{\pi} \int_{-a}^{a} K_1(x, s) \sigma^*_{yy}(s, 0, \xi) ds - \frac{2}{\pi} N_2(x), \quad |x| < \infty,
\end{aligned} \tag{62}$$

where $K_1(x,s)$ is given as follows:

$$K_1(x, s) = \int_0^\infty [L_1(\omega) - \Lambda_1] \cos(\omega s) \sin(\omega x) d\omega. \tag{63}$$

Taking into account Eqs. (30) and (31), one obtains the following Cauchy-type, singular integral equation in terms of the unknown function $p^*(x, \xi)$:

$$\frac{1}{\pi} \int_{-a}^{a} \frac{\Lambda_1}{s - x} p^*(s, \xi) ds + \frac{1}{\pi} \int_{-a}^{a} K_1(x, s) p^*(s, \xi) ds = \frac{2}{\pi} N_2(x), \quad |x| < a. \tag{64}$$

To make the stated problem complete, equilibrium condition (32) in the Laplace-transformed plane should be considered.

By introducing the following normalized quantities:

$$\begin{aligned}
&x = a\chi, \quad s = ar, \quad -a < (x, s) < a, \quad -1 < (\chi, r) < 1, \\
&p^*(x, \xi) = \varphi(\chi, \xi), \quad K_1(\chi, r) = aK_1(x, s), \quad N_2(\chi) = aN_2(x),
\end{aligned} \tag{65}$$

Eqs. (64) and (32) can be rewritten as follows:

$$\frac{1}{\pi}\int_{-1}^{1}\frac{\Lambda_1}{r-\chi}\varphi(r,\xi)dr+\frac{1}{\pi}\int_{-1}^{1}K_1(\chi,r)\varphi(r,\xi)dr=\frac{2}{\pi}N_0(\chi),\quad |\chi|<1, \tag{66}$$

$$\int_{-1}^{1}\varphi(r,\xi)dr=\frac{P}{\xi a}. \tag{67}$$

The solutions of Eqs. (66) and (67) can be expressed as (Erdogan and Gupta, 1972):

$$\varphi(r,\xi)=\frac{\Phi(r,\xi)}{\sqrt{1-r^2}},\quad \Phi(r,\xi)=\sum_{n=0}^{N}a_n(\xi)T_{2n}(r), \tag{68}$$

where $T_n(\cdot)$ are Chebyshev polynomials of the first kind and a_n ($n=0,1,\ldots,N$) are constants to be determined.

Considering the following integral formulas:

$$\frac{1}{\pi}\int_{-1}^{1}\frac{T_n(r)}{(r-\chi)\sqrt{1-r^2}}dr=\begin{cases}0, & n=0,\ |\chi|<1,\\ U_{n-1}(\chi) & n\geqslant 1,\ |\chi|<1,\\ -sgn(\chi)/\sqrt{\chi^2-1}\left[\chi-sgn(\chi)\sqrt{\chi^2-1}\right]^n & n\geqslant 0,\ |\chi|>1,\end{cases} \tag{69}$$

where $U_n(\cdot)$ are Chebyshev polynomials of the second kind and $sgn(\cdot)$ is the sign function, respectively, and inserting Eq. (68) into Eq. (66), one obtains:

$$\sum_{n=1}^{N}a_n\Lambda_1U_{2n-1}+\sum_{n=0}^{N}a_nH_n(\chi)=\frac{2}{\pi}N_2(\chi),\quad |\chi|<1, \tag{70}$$

where

$$H_n(\chi)=(-1)^n a\int_0^{\infty}[L_1(\omega)-\Lambda_1]J_{2n}(\omega\cdot a)\sin(\omega\cdot a\cdot\chi)d\omega, \tag{71}$$

where $J_m(\cdot)$ is the m-order Bessel function of the first kind.

Inserting Eq. (68) into Eq. (67) yields:

$$a_0=\frac{P}{\pi\xi a}. \tag{72}$$

The algebraic Eq. (70) can be solved numerically by the standard collocation technique. Thus, $\{a_n\}$ can be determined. The unknown function $p^*(x,\xi)$ in terms of a_n ($n=0,1,\ldots,N$) can be obtained as follows:

$$p^*(x,\xi)=\frac{1}{\sqrt{1-(x/a)^2}}\sum_{n=0}^{N}a_n(\xi)T_{2n}\left(\frac{x}{a}\right),\quad |x|<a. \tag{73}$$

The contact stress beneath the punch in the Laplace-transformed plane in terms of $p^*(x,\xi)$ can be obtained through Eq. (31).

The stress intensity factor at the end point of the punch in the Laplace-transformed plane can be defined as:

$$K_I^*=\lim_{x\to a^-}\sqrt{2(a-x)}\sigma_{yy}^*(x,0,\xi). \tag{74}$$

Then,

$$K_I^*=-\sqrt{a}\sum_{n=0}^{N}a_n. \tag{75}$$

6. Inverse Laplace transform

The numerical solutions of temperature, contact stress and stress intensity factor in the time domain can be obtained by employing the numerical inversion method of the Laplace transform (see Eq. (18)) proposed by Weeks (1966). Using Weeks' method, Davis and Martin (1979) found that excellent accuracy can be given for the inversion of a wide range of functions. This effective numerical inversion algorithm of the Laplace transform can be outlined as follows:

$$w(t)=e^{c_1t-\frac{t}{2c_2}}\sum_{m=1}^{M}b_mL_m\left(\frac{t}{c_2}\right), \tag{76}$$

where

$$b_m=\frac{2-\delta_{m,0}}{2c_2(M+1)}\sum_{n=1}^{M}\left\{Re[w^*(\xi_n)]-\cot\frac{z_n}{2}\cdot Im[w^*(\xi_n)t]\right\}\cos(n\cdot z_n), \tag{77}$$

$$z_n=\frac{\pi(2n+1)}{2(M+1)},\quad \xi_n=c_1+\frac{i}{2c_2}\cot\frac{z_n}{2}, \tag{78}$$

$$c_1=\frac{1}{t_{\max}},\quad c_2=\frac{t_{\max}}{M}, \tag{79}$$

where $Re[]$ and $Im[]$ denote the real part and the imaginary part, respectively, δ is the Kronecker delta and $t_{\max}$ is the maximum required value of the argument for the function $w()$. The accuracy of the numerical results is controlled by the value of M, which depends on $t_{\max}$.

7. Special cases

The following special cases are considered in the present investigation: (i) isothermal contact and (ii) infinite thickness.

7.1. Isothermal contact

By inspecting Eqs. (8) and (25), either the surrounding temperature $T_0(t)\to 0$ or the relative surface heat transfer coefficient $H_a\to 0$ will lead to the vanishing of the terms related to the temperature. Thus, thermal contact problems subjected to a transient convective heat supply may be reduced to static isothermal contact problems. Because in the expressions of all electric-mechanical quantities, the terms related to temperature vanish, Eq. (53) can be simplified as

$$M_j=\frac{(-1)^{1+j}F}{\omega}\frac{H_{1j}}{H} \tag{80}$$

Obviously, this result will make the derivations of isothermal contact problems more convenient.

7.2. Infinite layer thickness

In the case of $h\to\infty$, $\Theta_{mn}(\omega,y)=0$ ($m=1,2,3$, $n=4,5,6$) and $\Omega_{kl}(\omega,y)=0$ ($k=0,1,2,3$, $n=4,5,6$). Consequently, $K_1(x,s)$ defined in Eq. (63) is equal to zero.

In specific, the closed-form solutions can be obtained for the static isothermal contact problems in infinite piezoelectric materials indented by a rigid punch. By inspecting Eqs. (70) and (72), one obtains the contact pressure beneath the punch as follows (see Appendix B):

$$\sigma_{yy}(x,0)=-p(x)=-\frac{P}{\pi\sqrt{a^2-x^2}}. \tag{81}$$

Substituting Eq. (81) into Eq. (56), one can simplify Eq. (80) as:

$$M_j=\frac{(-1)^jP}{2\omega}\frac{H_{1j}}{H}J_0(\omega\cdot a)\quad (j=1,2,3), \tag{82}$$

where $J_0(\cdot)$ is a zero-order Bessel function of the first kind.

Inserting Eq. (82) into Eqs. (51) and (52) (where both the superscript $*$ and the second term on the right-hand side should be suppressed for the static isothermal contact problem) yields the following expressions of the stresses and electric displacement in a static state:

$$\sigma_{xx}=\frac{P}{\pi}\sum_{j=1}^{3}(-1)^j\frac{H_{1j}}{H}\Delta_{0j}(x,y),\quad \sigma_{yy}=\frac{P}{\pi}\sum_{j=1}^{3}(-1)^j\frac{H_{1j}}{H}\Delta_{1j}(x,y),$$
$$\sigma_{xy}=\frac{P}{\pi}\sum_{j=1}^{3}(-1)^j\frac{H_{1j}}{H}\Delta_{2j}(x,y),\quad D_y=\frac{P}{\pi}\sum_{j=1}^{3}(-1)^j\frac{H_{1j}}{H}\Delta_{3j}(x,y), \tag{83}$$

where the known functions $\Delta_{nj}(x,y)$ $(n=0,1,2,3, j=1,2,3)$ are given in Appendix A.

8. Numerical results

For further investigation, the piezoelectric ceramic is assumed to be Cadmium Selenide. The elastic constants are $c_{11}=7.41\times10^{10}$ N/m^2, $c_{13}=3.93\times10^{10}$ N/m^2, $c_{33}=8.36\times10^{10}$ N/m^2, $c_{44}=1.32\times10^{10}$ N/m^2. The thermal conductivity coefficients are $k_1=9$ W/km, $k_3=9$ W/km. The density is $\rho=5.816\times10^3$ kg/m^3. The nonzero piezoelectric constants are $e_{31}=-0.160$ C/m^2, $e_{33}=0.347$ C/m^2, $e_{15}=-0.138$ C/m^2. The dielectric coefficients are $\epsilon_{11}=0.825\times10^{-10}$ C/Vm, $\epsilon_{33}=0.902\times10^{-10}$ C/Vm. The thermal stress coefficients are $\lambda_{11}=0.621\times10^6$ N/km^2, $\lambda_{33}=0.551\times10^6$ N/km^2. The pyroelectric constant is $\beta_3=-2.94\times10^{-6}$ C/km^2.

The Fourier number is denoted by $\tau=D_2\cdot t/c^2$, i.e., the dimensionless time. The closed-form solution in the special case that $H_a\to0$ and $h\to\infty$ in Section 7.2 is employed to verify the validity of the present work.

In the thermal contact problem, the separation of the contacting surfaces might occur and the contact stress $(\sigma_{yy}(x,0,t)=-p(x,t), |x|<a)$ might become positive and tensile inside the contact region due to the excessive thermal flux generated by the excessive, large surrounding temperature and the large surface heat transfer coefficient. A lower surrounding temperature and small surface heat transfer coefficient below certain levels are selected to avoid contact surface damage.

To conduct the foregoing analysis, the numerical parameters of heat conduction and shape are presented as follows:

$$H_a=1,\quad T_0=1,\quad f_0\left(\frac{x}{a}\right)=\begin{cases}1-\frac{x^2}{x_0^2}, & |x|\leqslant x_0,\\ 0, & |x|>x_0,\end{cases} \tag{84}$$

where x_0 stands for a half of the heating length.

In what follows, numerical results $(x_0=a)$ are obtained to illustrate the effects of the dimensionless time and the layer thickness on the temperature distribution, stress distribution and stress intensity factors beneath the punch foundation.

8.1. Temperature distribution

Fig. 2(a) and (b) show the distribution of the normalized temperature $T(x,-0.001,\tau)/T_0$ along the line $(y/a=-0.001)$ parallel to the surface with the varying of the dimensionless time τ. Here, T_0 is the reference temperature. As shown in Fig. 2, the temperature beneath the punch rises as the time proceeds and reaches a steady-state value gradually. By increasing the layer thickness, the temperature beneath the punch reaches the steady-state value more quickly. At any moment, the peak value of the normalized temperature occurs at the punch center. Fig. 2 also indicates that the temperature beneath the punch becomes more pronounced as the piezoelectric strip becomes thinner.

As mentioned in Fig. 2, the peak value of the normalized temperature beneath the punch occurs at the punch center. The distribution of the normalized temperature $T(0,y,\tau)/T_0$ along the punch axis $(x/a=0)$ with the variation of the dimensionless time τ is concerned and is illustrated in Fig. 3(a) and (b). It can be seen that the temperature along the punch axis rises and reaches a steady-state value as time increases. The temperature along the punch axis may reach the steady-state value more quickly as the layer thickness increases. The temperature along the punch axis becomes higher as the piezoelectric strip becomes thinner. As the relative distance of a point from the heated lower surface increases, the corresponding temperature decreases.

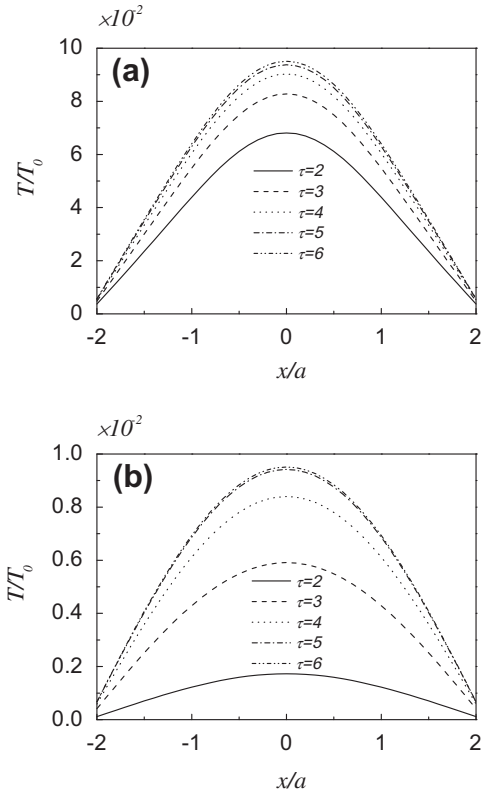

Fig. 2. Distribution of the normalized temperatures $T(x,-0.001,\tau)/T_0$ beneath the punch with different dimensionless times τ. (a) $h/a=1$, (b) $h/a=3$.

8.2. Surface contact stress distribution beneath the punch

Contact surface damage might occur due to the highly concentrated stress. Thus, great interest is focused on the contact stress distribution beneath the punch in general contact problems.

Fig. 4(a) and (b) show the distribution of the normalized contact stress $\sigma_{yy}(x,0,\tau)/\sigma_0$ beneath the punch with the variation of the dimensionless time τ, where $\sigma_0=P/2a$ is the average contact pressure. Fig. 4 clearly shows that, at any moment, the magnitude of the normalized contact stress increases with increasing the distance of the point from the punch center and becomes infinite at the punch edges. Thus, a near-edge response, i.e., a severe stress concentration does exist around the punch edge. The magnitude of the normalized contact stress decreases with decreasing layer thickness. The normalized contact stress reaches a steady-state value more quickly as the layer thickness increases. At any moment, the normalized surface contact stress is compressive beneath the punch.

In addition, Fig. 4 also illustrates that there exists a critic value α_0 (here, $\alpha_0\approx0.72$) that divides the normalized interval $(-1,1)$ beneath the punch into two parts: (i) $|x/a|<\alpha_0$, which may be characterized as the near-punch-center interval; (ii) $|x/a|>\alpha_0$, which may be characterized as the near-punch-edge interval. The magnitude of the normalized contact stress increases as time proceeds when $|x/a|<\alpha_0$ while the magnitude of the normalized surface contact stress decreases as time proceeds when $|x/a|>\alpha_0$. This phenomenon is further revealed in Fig. 5.

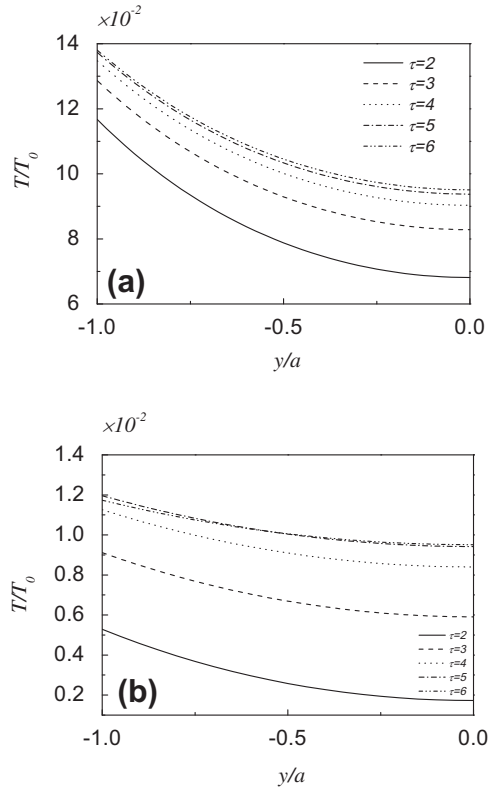

Fig. 3. Distribution of the normalized temperatures $T(0,y,\tau)/T_0$ along the punch axis ($x/a = 0$) with different dimensionless times τ. (a) $h/a = 1$, (b) $h/a = 3$.

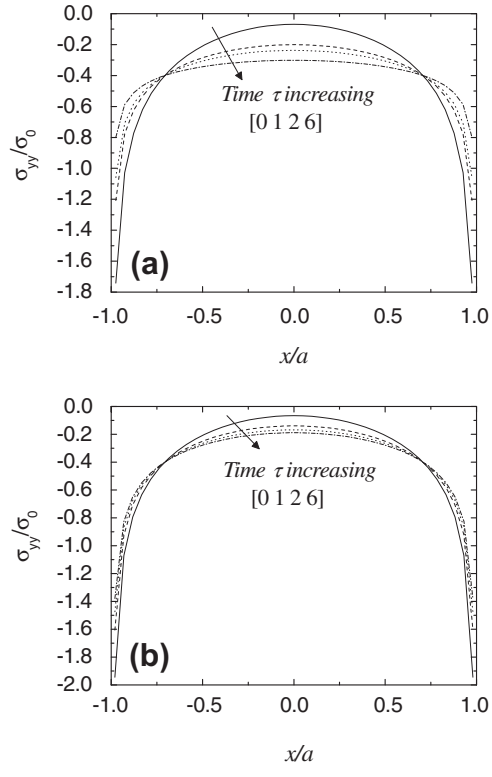

Fig. 4. Distribution of the normalized contact stress $\sigma_{yy}(x,0,\tau)/\sigma_0$ beneath the punch with different dimensionless times τ. (a) $h/a = 1$, (b) $h/a = 3$.

Fig. 5(a) confirms that the magnitude of the normalized surface contact stress increases from its initial minimum value to a steady value as time proceeds when $|x/a| < \alpha_0$. Fig. 5(b) reassures that

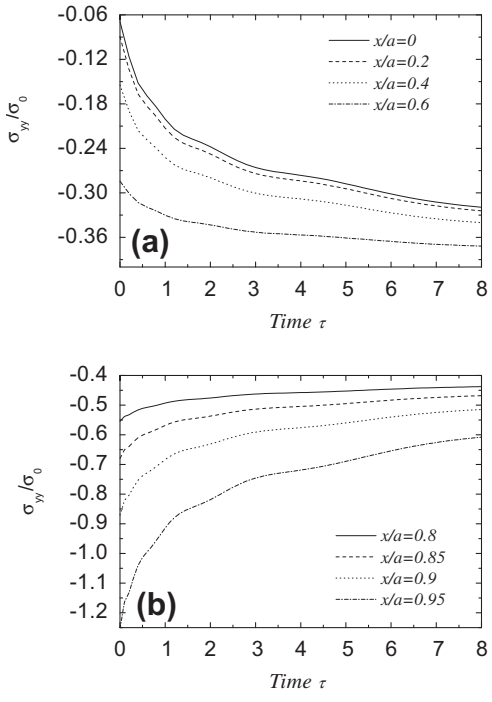

Fig. 5. Distribution of the normalized contact stress $\sigma_{yy}(x,0,\tau)/\sigma_0$ beneath the punch, $h/a = 1$. (a) $|x/a| < \alpha_0$, (b) $|x/a| > \alpha_0$.

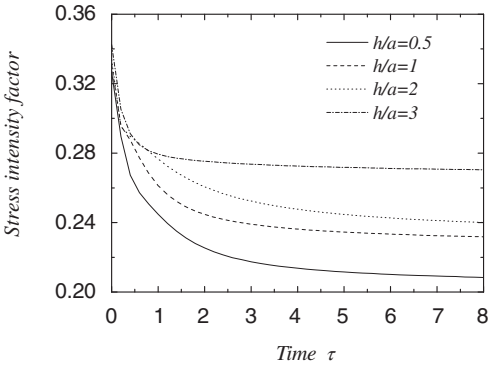

Fig. 6. Influences of the layer thickness h/a on the normalized stress intensity factor with the different dimensionless times τ.

when $|x/a| > \alpha_0$, the magnitude of the normalized surface contact stress decreases from its initial maximum value to a steady value as time proceeds. Further more, Fig. 5(a) also depicts that the magnitude of the normalized contact stress decreases as the point becomes closer to the punch center while Fig. 5(b) illustrates that the normalized contact stress increases as the point becomes closer to the punch edge.

8.3. Stress intensity factor at the punch edge

Fig. 6 shows the effects of the layer thickness h/a on the normalized stress intensity factor $K_I(1)/K_0$ as time varies, where $K_0 = -P/\sqrt{a}$. Fig. 6 depicts that the normalized stress intensity factor decreases from its initial maximum value to a steady value as the dimensionless time τ proceeds. The normalized stress intensity factor decreases as the layer thickness increases. The normalized stress intensity factor reaches a steady-state value more quickly with increasing layer thickness.

Table 1
Results of $\varepsilon_p/\varepsilon_0$, $\varepsilon_t/\varepsilon_0$ and $\varepsilon_t/\varepsilon_p$ on the surface $y = 0$ when $h/a = 3$.

$\frac{x}{a}$	$\tau = 1$			$\tau = 2$			$\tau = 3$		
	$\frac{\varepsilon_p}{\varepsilon_0}$	$\frac{\varepsilon_t}{\varepsilon_0}$	$\frac{\varepsilon_t}{\varepsilon_p}$	$\frac{\varepsilon_p}{\varepsilon_0}$	$\frac{\varepsilon_t}{\varepsilon_0}$	$\frac{\varepsilon_t}{\varepsilon_p}$	$\frac{\varepsilon_p}{\varepsilon_0}$	$\frac{\varepsilon_t}{\varepsilon_0}$	$\frac{\varepsilon_t}{\varepsilon_p}$
0	4.8809	0.2188	4.48%	5.5429	0.6781	12.23%	5.49	0.7152	13.03%
0.1	4.8239	0.2181	4.52%	5.4747	0.6762	12.35%	5.422	0.7131	13.15%
0.2	4.6542	0.2161	4.64%	5.2714	0.6704	12.72%	5.2197	0.707	13.54%
0.3	4.3757	0.2129	4.86%	4.9379	0.6607	13.38%	4.8877	0.6968	14.26%
0.4	3.995	0.2083	5.21%	4.482	0.6472	14.44%	4.4338	0.6826	15.4%
0.5	3.5207	0.2026	5.75%	3.9143	0.6301	16.1%	3.8686	0.6646	17.18%
0.6	2.964	0.1956	6.6%	3.2481	0.6094	18.76%	3.2054	0.6428	20.05%

8.4. Thermal-piezoelectric strain

In this subsection, to gain a deep insight into the thermal contact problem in piezoelectric materials, a comparison of the thermal strain and the piezoelectric strain is presented. The strain can be evaluated from the following relation:

$$\varepsilon_{xx} = \frac{c_{33}\sigma_{xx} - c_{13}\sigma_{yy} + (c_{33}e_{31} - c_{13}e_{33})E_y}{c_{11}c_{33} - (c_{13}t)^2} + \frac{(c_{33}\lambda_{11} - c_{13}\lambda_{33})T}{c_{11}c_{33} - (c_{13})^2}. \tag{85}$$

On the right-hand side of Eq. (85), the first term is the piezoelectric strain and may be denoted as ε_p, which is generated by the electric-mechanical loading. The second term is the thermal strain and may be denoted as ε_t, which is generated by the thermal loading.

The results of $\varepsilon_p/\varepsilon_0$, $\varepsilon_t/\varepsilon_0$ and $\varepsilon_t/\varepsilon_p$ ($\varepsilon_0 = 100P/(a \cdot c_{44})$) on the surface $y = 0$ are presented in Table 1. Table 1 clearly shows that for various positions x/a and dimensionless time τ, the main contribution to the total strain originates from the piezoelectric strain ε_p for the present lower reference temperature $T_0 = 1$ (see Eq. (84)). As seen from Eq. (85), the thermal strains could be much higher if a higher reference temperature T_0 is used in the computations.

9. Conclusions

A transient thermal contact investigation has been performed for a finite-thickness piezoelectric strip under the coupling actions of a rigid, flat punch and a convective heat supply by the real fundamental solution-based method, which can lead to real solutions to thermo-electro-mechanical quantities. The Laplace transform and Fourier sine and cosine transforms were employed in reducing the mixed boundary value problem to a Cauchy-type, singular integral equation in the Laplace-transformed plane. An effective numerical inversion algorithm of the Laplace transform was implemented to get the solution in the time domain. Detailed analyses were conducted to reveal the effects of the dimensionless time and the layer thickness on the distribution of temperature, contact stress beneath the punch and stress intensity factor at the punch edge. A thermal-piezoelectric strain analysis was also made.

The Numerical results show the following: (i) The temperature rises as time proceeds, gradually reaching a steady-state value and the peak value occurs at the punch center. (ii) The temperature beneath the punch reaches a steady-state value more quickly by increasing the layer thickness. (iii) At any moment, the normalized surface contact stress is compressive beneath the punch for the present loadings and a near-edge response, i.e., a severe stress concentration does exist around the punch edge. (iv) The magnitude of the normalized contact stress decreases by decreasing the layer thickness. The normalized contact stress reaches a steady-state value more quickly as the layer thickness increases. (v) The normalized stress intensity factor decreases from its initial maximum value to a steady value as the dimensionless time τ proceeds and reaches a steady-state value more quickly as the layer thickness increases. The normalized stress intensity factor decreases as the layer thickness increases. (vi) The total strain is the sum of the piezoelectric strain and thermal strain. Thermal strain greatly depends on the reference temperature.

These results provide the very useful information for interpreting the behaviors of the piezoelectric materials working in a highly complex environment.

Acknowledgements

The authors are grateful for the reviewers' generous and valuable suggestions.

Appendix A

1. Expressions of the matrices appearing in Eq. (49)

$$a_{11}^{(k)} = c_{11} - (n_k)^2 c_{44}, \quad a_{12}^{(k)} = n_k(c_{13} + c_{44}), \quad a_{13}^{(k)} = n_k(e_{31} + e_{15}),$$
$$a_{21}^{(k)} = n_k(c_{13} + c_{44}), \quad a_{22}^{(k)} = -c_{44} + (n_k)^2 c_{33}, \quad a_{23}^{(k)} = -e_{15} + (n_k)^2 e_{33},$$
$$a_{31}^{(k)} = n_k(e_{31} + e_{15}), \quad a_{32}^{(k)} = -e_{15} + (n_k)^2 e_{33}, \quad a_{33}^{(k)} = \in_{11} - (n_k)^2 \in_{33}. \tag{A.1}$$

2. Expressions of $\Omega_{nj}(\omega, y)$ ($n = 0,1,2,3$, $j = 1,\ldots,6$) appearing in Eqs. (51) and (52)For Case A:

$$\Omega_{0j}(\omega, y) = [c_{11} + c_{13}\eta_j f(\eta_j) + e_{31}\eta_j g(\eta_j)]e^{\omega\eta_j y}, \quad j = 1,2,3,$$
$$\Omega_{0j}(\omega, y) = [-c_{11} - c_{13}\eta_{j-3} f(\eta_{j-3}) - e_{31}\eta_{j-3} g(\eta_{j-3})]e^{-\omega\eta_{j-3} y}, \quad j = 4,5,6, \tag{A.2}$$

$$\Omega_{1j}(\omega, y) = [c_{13} + c_{33}\eta_j f(\eta_j) + e_{33}\eta_j g(\eta_j)]e^{\omega\eta_j y}, \quad j = 1,2,3,$$
$$\Omega_{1j}(\omega, y) = [-c_{13} - c_{33}\eta_{j-3} f(\eta_{j-3}) - e_{33}\eta_{j-3} g(\eta_{j-3})]e^{-\omega\eta_{j-3} y}, \quad j = 4,5,6, \tag{A.3}$$

$$\Omega_{2j}(\omega, y) = \{c_{44}[\eta_j - f(\eta_j)] - e_{15} g(\eta_j)\}e^{\omega\eta_j y}, \quad j = 1,2,3,$$
$$\Omega_{2j}(\omega, y) = \{c_{44}[\eta_{j-3} - f(\eta_{j-3})] - e_{15} g(\eta_{j-3})\}e^{-\omega\eta_{j-3} y}, \quad j = 4,5,6, \tag{A.4}$$

$$\Omega_{3j}(\omega, y) = [e_{31} + e_{33}\eta_j f(\eta_j) - \in_{33}\eta_j g(\eta_j)]e^{\omega\eta_j y}, j = 1,2,3,$$
$$\Omega_{3j}(\omega, y) = [-e_{31} - e_{33}\eta_{j-3} f(\eta_{j-3}) + \in_{33}\eta_{j-3} g(\eta_{j-3})]e^{-\omega\eta_{j-3} y}, \quad j = 4,5,6, \tag{A.5}$$

For Case B:

$$(\Omega_{01}(\omega, y) = [c_{11} + c_{13}\tau_0 f(\tau_0) + e_{31}\tau_0 g(\tau_0)]e^{\omega\tau_0 y},$$
$$\Omega_{02}(\omega, y) = \{[c_{11} + c_{13}(\mu\Gamma_1 - \nu\Delta_1) + e_{31}(\mu\Gamma_2 - \nu\Delta_2)]\cos(\omega\nu y) - [c_{13}(\mu\Delta_1 + \nu\Gamma_1) + e_{31}(\mu\Delta_2 + \nu\Gamma_2)]\sin(\omega\nu y)\}e^{\omega\mu y}, \tag{A.6}$$

$$\Omega_{03}(\omega,y)=\{[c_{13}(\mu\Delta_1+\nu\Gamma_1)+e_{31}(\mu\Delta_2+\nu\Gamma_2)]\cos(\omega\nu y)+[c_{11}+c_{13}(\mu\Gamma_1-\nu\Delta_1)+e_{31}(\mu\Gamma_2-\nu\Delta_2)]\sin(\omega\nu y)\}e^{\omega\mu y},$$

$$\Omega_{04}(\omega,y)=[-c_{11}-c_{13}\tau_0 f(\tau_0)-e_{31}\tau_0 g(\tau_0)]e^{-\omega\tau_0 y},$$

$$\Omega_{05}(\omega,y)=\{[c_{11}+c_{13}(\mu\Gamma_1-\nu\Delta_1)+e_{31}(\mu\Gamma_2-\nu\Delta_2)]\cos(\omega\nu y)+[c_{13}(\mu\Delta_1+\nu\Gamma_1)+e_{31}(\mu\Delta_2+\nu\Gamma_2)]\sin(\omega\nu y)\}e^{-\omega\mu y},$$

$$\Omega_{06}(\omega,y)=\{[c_{13}(\mu\Delta_1+\nu\Gamma_1)+e_{31}(\mu\Delta_2+\nu\Gamma_2)]\cos(\omega\nu y)-[c_{11}+c_{13}(\mu\Gamma_1-\nu\Delta_1)+e_{31}(\mu\Gamma_2-\nu\Delta_2)]\sin(\omega\nu y)\}e^{-\omega\mu y},$$

$$\Omega_{11}(\omega,y)=[c_{13}+c_{33}\tau_0 f(\tau_0)+e_{33}\tau_0 g(\tau_0)]e^{\omega\tau_0 y},$$

$$\Omega_{12}(\omega,y)=\{[c_{13}+c_{33}(\mu\Gamma_1-\nu\Delta_1)+e_{33}(\mu\Gamma_2-\nu\Delta_2)]\cos(\omega\nu y)-[c_{33}(\mu\Delta_1+\nu\Gamma_1)+e_{33}(\mu\Delta_2+\nu\Gamma_2)]\sin(\omega\nu y)\}e^{\omega\mu y},$$

$$\Omega_{13}(\omega,y)=\{[c_{33}(\mu\Delta_1+\nu\Gamma_1)+e_{33}(\mu\Delta_2+\nu\Gamma_2)]\cos(\omega\nu y)+[c_{13}+c_{33}(\mu\Gamma_1-\nu\Delta_1)+e_{33}(\mu\Gamma_2-\nu\Delta_2)]\sin(\omega\nu y)$$

$$\Omega_{14}(\omega,y)=[-c_{13}-c_{33}\tau_0 f(\tau_0)-e_{33}\tau_0 g(\tau_0)]e^{-\omega\tau_0 y},\tag{A.7}$$

$$\Omega_{15}(\omega,y)=\{[c_{13}+c_{33}(\mu\Gamma_1-\nu\Delta_1)+e_{33}(\mu\Gamma_2-\nu\Delta_2)]\cos(\omega\nu y)+[c_{33}(\mu\Delta_1+\nu\Gamma_1)+e_{33}(\mu\Delta_2+\nu\Gamma_2)]\sin(\omega\nu y)\}e^{-\omega\mu y},$$

$$\Omega_{16}(\omega,y)=\{[c_{33}(\mu\Delta_1+\nu\Gamma_1)+e_{33}(\mu\Delta_2+\nu\Gamma_2)]\cos(\omega\nu y)-[c_{13}+c_{33}(\mu\Gamma_1-\nu\Delta_1)+e_{33}(\mu\Gamma_2-\nu\Delta_2)]\sin(\omega\nu y)\}e^{-\omega\mu y},$$

$$\Omega_{21}(\omega,y)=\{c_{44}[\tau_0-f(\tau_0)]-e_{15}g(\tau_0)\}e^{\omega\tau_0 y},$$

$$\Omega_{22}(\omega,y)=\{[c_{44}(\mu-\Gamma_1)-e_{15}\Gamma_2]\cos(\omega\nu y)+[c_{44}(-\nu+\Delta_1)+e_{15}\Delta_2]\sin(\omega\nu Y)\}e^{\omega\mu y},$$

$$\Omega_{23}(\omega,y)=\{[c_{44}(\nu-\Delta_1)-e_{15}\Delta_2]\cos(\omega\nu y)+[c_{44}(\mu-\Gamma_1)-e_{15}\Gamma_2]\sin(\omega\nu y)\}e^{\omega\mu y},$$

$$\Omega_{24}(\omega,y)=\{c_{44}[\tau_0-f(\tau_0)]-e_{15}g(\tau_0)\}e^{-\omega\tau_0 y},\tag{A.8}$$

$$\Omega_{25}(\omega,y)=\{[c_{44}(-\mu+\Gamma_1)+e_{15}\Gamma_2]\cos(\omega\nu y)+[c_{44}(-\nu+\Delta_1)+e_{15}\Delta_2]\sin(\omega\nu y)\}e^{-\omega\mu y},$$

$$\Omega_{26}(\omega,y)=\{[c_{44}(-\nu+\Delta_1)+e_{15}\Delta_2]\cos(\omega\nu y)+[c_{44}(\mu-\Gamma_1)-e_{15}\Gamma_2]\sin(\omega\nu y)\}e^{-\omega\mu y},$$

$$\Omega_{31}(\omega,y)=[e_{31}+e_{33}\tau_0 f(\tau_0)-\in_{33}\tau_0 g(\tau_0)]e^{\omega\tau_0 y},\tag{A.9}$$

$$\Omega_{32}(\omega,y)=\{[e_{31}+e_{33}(\mu\Gamma_1-\nu\Delta_1)-\in_{33}(\mu\Gamma_2-\nu\Delta_2)]\cos(\omega\nu y)-[e_{33}(\mu\Delta_1+\nu\Gamma_1)-\in_{33}(\mu\Delta_2+\nu\Gamma_2)]\sin(\omega\nu y)\}e^{\omega\mu y},$$

$$\Omega_{33}(\omega,y)=\{[e_{33}(\mu\Delta_1+\nu\Gamma_1)-\in_{33}(\mu\Delta_2+\nu\Gamma_2)]\cos(\omega\nu y)+[e_{31}+e_{33}(\mu\Gamma_1-\nu\Delta_1)-\in_{33}(\mu\Gamma_2-\nu\Delta_2)]\sin(\omega\nu y)$$

$$\Omega_{34}(\omega,y)=[-e_{31}-e_{33}\tau_0 f(\tau_0)+\in_{33}\tau_0 g(\tau_0)]e^{-\omega\tau_0 y},$$

$$\Omega_{35}(\omega,y)=\{[e_{31}+e_{33}(\mu\Gamma_1-\nu\Delta_1)-\in_{33}(\mu\Gamma_2-\nu\Delta_2)]\cos(\omega\nu y)+[e_{33}(\mu\Delta_1+\nu\Gamma_1)-\in_{33}(\mu\Delta_2+\nu\Gamma_2)]\sin(\omega\nu y)\}e^{-\omega\mu y},$$

$$\Omega_{36}(\omega,y)=\{[e_{33}(\mu\Delta_1+\nu\Gamma_1)-\in_{33}(\mu\Delta_2+\nu\Gamma_2)]\cos(\omega\nu y)-[e_{31}+e_{33}(\mu\Gamma_1-\nu\Delta_1)-\in_{33}(\mu\Gamma_2-\nu\Delta_2)]\sin(\omega\nu y)\}e^{-\omega\mu y},$$

3. Expressions of $T_{nk}(\omega)$ ($n=0,1,2,3$, $k=1,2$) appearing in Eqs. (51) and (52)

$$\begin{aligned}T_{0k}&=c_{11}F_{1k}+c_{13}n_kF_{2k}+e_{31}n_kF_{3k}-\lambda_{11},\\ T_{1k}&=c_{13}F_{1k}+c_{33}n_kF_{2k}+e_{33}n_kF_{3k}-\lambda_{33},\\ T_{2k}&=c_{44}(n_kF_{1k}-F_{2k})-e_{15}F_{3k},\\ T_{3k}&=e_{31}F_{1k}+e_{33}n_kF_{2k}-\in_{33}n_kF_{3k}+\beta_3.\end{aligned}\tag{A.10}$$

4. Expressions of $\Delta_{nj}(x,y)$ ($n=0,1,2,3$, $j=1,2,3$) appearing in Eq. (83)

For Case A:

$$\Delta_{0j}(x,y)=\left[c_{11}+c_{13}\eta_j f(\eta_j)+e_{31}\eta_j g(\eta_j)\right]\frac{\sqrt{\lambda_{2j}^2-x^2}}{\lambda_{2j}^2-\lambda_{1j}^2},\quad j=1,2,3,\tag{A.11}$$

$$\Delta_{1j}(x,y)=\left[c_{13}+c_{33}\eta_j f(\eta_j)+e_{33}\eta_j g(\eta_j)\right]\frac{\sqrt{\lambda_{2j}^2-x^2}}{\lambda_{2j}^2-\lambda_{1j}^2},\quad j=1,2,3,\tag{A.12}$$

$$\Delta_{2j}(x,y)=\{c_{44}[\eta_j-f(\eta_j)]-e_{15}g(\eta_j)\}\frac{\sqrt{x^2-\lambda_{1j}^2}}{\lambda_{2j}^2-\lambda_{1j}^2},\quad j=1,2,3,\tag{A.13}$$

$$\Delta_{3j}(x,y)=\left[e_{31}+e_{33}\eta_j f(\eta_j)-\in_{33}\eta_j g(\eta_j)\right]\frac{\sqrt{\lambda_{2j}^2-x^2}}{\lambda_{2j}^2-\lambda_{1j}^2},\quad j=1,2,3,\tag{A.14}$$

where

$$\lambda_{1j}=\frac{1}{2}\left(\sqrt{(x+a)^2+(\eta_j y)^2}-\sqrt{(x-a)^2+(\eta_j y)^2}\right),\quad j=1,2,3,\tag{A.15}$$

$$\lambda_{2j}=\frac{1}{2}\left(\sqrt{(x+a)^2+(\eta_j y)^2}+\sqrt{(x-a)^2+(\eta_j y)^2}\right),\quad j=1,2,3.\tag{A.16}$$

For Case B:

$$\Delta_{01}(x,y)=[c_{11}+c_{13}\tau_0 f(\tau_0)+e_{31}\tau_0 g(\tau_0)]\frac{\sqrt{\gamma_2^2-x^2}}{\gamma_2^2-\gamma_1^2},\tag{A.17}$$

$$\Delta_{02}(x,y)=\frac{1}{2}\{[c_{11}+c_{13}(\mu\Gamma_1-\nu\Delta_1)+e_{31}(\mu\Gamma_2-\nu\Delta_2)][\Lambda_{11}(x,y)+\Lambda_{12}(x,y)]-[c_{13}(\mu\Delta_1+\nu\Gamma_1)+e_{31}(\mu\Delta_2+\nu\Gamma_2)][\Lambda_{21}(x,y)+\Lambda_{22}(x,y)]\},$$

$$\Delta_{03}(\omega,y)=\frac{1}{2}\{[c_{13}(\mu\Delta_1+\nu\Gamma_1)+e_{31}(\mu\Delta_2+\nu\Gamma_2)][\Lambda_{11}(x,y)+\Lambda_{12}(x,y)]+[c_{11}+c_{13}(\mu\Gamma_1-\nu\Delta_1)+e_{31}(\mu\Gamma_2-\nu\Delta_2 t)][\Lambda_{21}(x,y)+\Lambda_{22}(x,y)]\},$$

$$\Delta_{11}(x,y)=[c_{13}+c_{33}\tau_0 f(\tau_0)+e_{33}\tau_0 g(\tau_0)]\frac{\sqrt{\gamma_2^2-x^2}}{\gamma_2^2-\gamma_1^2},$$

$$\Delta_{12}(x,y)=\frac{1}{2}\{[c_{13}+c_{33}(\mu\Gamma_1-\nu\Delta_1)+e_{33}(\mu\Gamma_2-\nu\Delta_2 t)][\Lambda_{11}(x,y)+\Lambda_{12}(x,y)]-[c_{33}(\mu\Delta_1+\nu\Gamma_1)+e_{33}(\mu\Delta_2+\nu\Gamma_2)][\Lambda_{21}(x,y)+\Lambda_{22}(x,y)]\},$$

$$\Delta_{13}(x,y)=\frac{1}{2}\{[c_{33}(\mu\Delta_1+\nu\Gamma_1)+e_{33}(\mu\Delta_2+\nu\Gamma_2)][\Lambda_{11}(x,y)+\Lambda_{12}(x,y)]+[c_{13}+c_{33}(\mu\Gamma_1-\nu\Delta_1)+e_{33}(\mu\Gamma_2-\nu\Delta_2 t)][\Lambda_{21}(x,y)+\Lambda_{22}(x,y)]\},$$

$$\Delta_{21}(x,y)=\{c_{44}[\tau_0-f(\tau_0)]-e_{15}g(\tau_0)\}\frac{\sqrt{x^2-\gamma_1^2}}{\gamma_2^2-\gamma_1^2},$$

$$\begin{aligned}\Delta_{22}(x,y)=&\frac{1}{2}\{[c_{44}\mu-\Gamma_1)-e_{15}\Gamma_2][\Lambda_{21}(x,y)-\Lambda_{22}(x,y)]\\&+[c_{44}(-\nu+\Delta_1)+e_{15}\Delta_2][-\Lambda_{11}(x,y)+\Lambda_{12}(x,y)]\},\end{aligned}\quad(A.19)$$

$$\begin{aligned}\Delta_{23}(x,y)=&\frac{1}{2}\{[c_{44}(\nu-\Delta_1)-e_{15}\Delta_2][\Lambda_{21}(x,y)-\Lambda_{22}(x,y)]\\&+[c_{44}\mu-\Gamma_1)-e_{15}\Gamma_2][-\Lambda_{11}(x,y)+\Lambda_{12}(x,y)]\},\end{aligned}$$

$$\Delta_{31}(x,y)=[e_{31}+e_{33}\tau_0 f(\tau_0)-\in_{33}\tau_0 g(\tau_0)]\frac{\sqrt{\gamma_2^2-x^2}}{\gamma_2^2-\gamma_1^2},$$

$$\begin{aligned}\Delta_{32}(x,y)=&\frac{1}{2}\{[e_{31}+e_{33}(\mu\Gamma_1-\nu\Delta_1)-\in_{33}(\mu\Gamma_2-\nu\Delta_2 t)][\Lambda_{11}(x,y)+\Lambda_{12}(x,y)]\\&-[e_{33}(\mu\Delta_1+\nu\Gamma_1)-\in_{33}(\mu\Delta_2+\nu\Gamma_2)][\Lambda_{21}(x,y)+\Lambda_{22}(x,y)]\},\end{aligned}\quad(A.20)$$

$$\begin{aligned}\Delta_{33}(x,y)=&\frac{1}{2}\{[e_{33}(\mu\Delta_1+\nu\Gamma_1)-\in_{33}(\mu\Delta_2+\nu\Gamma_2)][\Lambda_{11}(x,y)+\Lambda_{12}(x,y)]\\&+[e_{31}+e_{33}(\mu\Gamma_1-\nu\Delta_1)-\in_{33}(\mu\Gamma_2-\nu\Delta_2 t)][\Lambda_{21}(x,y)+\Lambda_{22}(x,y)]\},\end{aligned}$$

where

$$\gamma_1=\frac{1}{2}\left(\sqrt{(x+a)^2+(\tau_0 y)^2}-\sqrt{(x-a)^2+(\tau_0 y)^2}\right),\quad(A.21)$$

$$\gamma_2=\frac{1}{2}\left(\sqrt{(x+a)^2+(\tau_0 y)^2}+\sqrt{(x-a)^2+(\tau_0 y)^2}\right),\quad(A.22)$$

$$\Lambda_{11}(x,y)=\frac{\sqrt{\gamma_{12}^2-x_1^2}}{\gamma_{12}^2-\gamma_{11}^2},\quad \Lambda_{12}(x,y)=\frac{\sqrt{\gamma_{22}^2-x_2^2}}{\gamma_{22}^2-\gamma_{21}^2},\quad(A.23)$$

$$\Lambda_{21}(x,y)=\frac{\sqrt{x_1^2-\gamma_{11}^2}}{\gamma_{12}^2-\gamma_{11}^2},\quad \Lambda_{22}(x,y)=\frac{\sqrt{x_2^2-\gamma_{21}^2}}{\gamma_{22}^2-\gamma_{21}^2}.$$

Here,

$$\gamma_{11}=\frac{1}{2}\left(\sqrt{(x_1+a)^2+(\mu y)^2}-\sqrt{(x_1-a)^2+(\mu y)^2}\right),\quad(A.24)$$

$$\gamma_{12}=\frac{1}{2}\left(\sqrt{(x_1+a)^2+(\mu y)^2}+\sqrt{(x_1-a)^2+(\mu y)^2}\right),\quad(A.25)$$

$$\gamma_{21}=\frac{1}{2}\left(\sqrt{(x_2+a)^2+(\mu y)^2}-\sqrt{(x_2-a)^2+(\mu y)^2}\right),\quad(A.26)$$

$$\gamma_{22}=\frac{1}{2}\left(\sqrt{(x_2+a)^2+(\mu y)^2}+\sqrt{(x_2-a)^2+(\mu y)^2}\right),\quad(A.27)$$

$$x_1=\nu y+x,\quad x_2=\nu y-x.\quad(A.28)$$

Appendix B. Derivation of Eq. (81)

For the static isothermal contact problems in the infinite piezoelectric materials indented by a rigid flat punch, $p(x,t)$ degenerates to $p(x)$. In Eq. (64), the integral kernel is $K_1(x,s)=0$ and the temperature related term is $N_2(x)=0$. By introducing the normalized quantities in analogy with those in Eq. (65), one can rewrite Eqs. (66) and (67) as follows:

$$\frac{1}{\pi}\int_{-1}^{1}\frac{L_1}{r-\chi}\varphi(r)dr=0,\quad |\chi|<1,\quad(B.1)$$

$$\int_{-1}^{1}\varphi(r)dr=\frac{P}{a}.\quad(B.2)$$

Considering Eqs. (68) (where ξ should be suppressed) and (69), one may rewrite Eqs. (B1) and (B2) as follows:

$$\sum_{n=1}^{N}a_n L_1 U_{2n-1}=0,\quad(B.3)$$

$$a_0=\frac{P}{\pi a}.\quad(B.4)$$

Because Chebyshev polynomials of the second kind $U_n(\cdot)$ are linearly independent,

$$a_n=0,\quad n=1,2,\ldots\quad(B.5)$$

Thus, only a_0 (Eq. (B.4)) remains non-zero. Considering Eq. (68) (where ξ should be suppressed), one obtains Eq. (81).

References

Ashida, F., Tauchert, T.R., 2001. Transient response of a piezothermoelastic circular disk under axisymmetric heating. Acta Mech. 128, 1–14.

Chandrasekharaiah, D.S., 1988. A generalized linear thermoelasticity theory for piezoelectric media. Acta Mech. 71, 39–49.

Chen, W.Q., 2000. On piezoelectric contact problem for a smooth punch. Int. J. Solids Struct. 37, 2331–2340.

Chen, Z.R., Yu, S.W., 2005. Micro-scale adhesive contact of a spherical rigid punch on a piezoelectric half-space. Compos. Sci. Technol. 65, 1372–1381.

Choi, J.S., Ashida, F., Noda, N., 1997. Control of thermally induced elastic displacement of an isotropic structural plate bonded to a piezoelectric ceramic plate. Acta Mech. 122, 49–63.

Davis, B., Martin, B., 1979. Numerical inversion of the laplace transforms: a survey and comparison of methods. J. Comput. Phys. 33, 1–32.

Ding, H.J., Chen, B., Liang, J., 1996. General solutions for coupled equations for piezoelectric media. Int. J. Solids Struct. 33, 2283–2298.

Ding, H.J., Hou, P.F., Gou, F.L., 2000. The elastic and electric fields for three-dimensional contact for transversely isotropic piezoelectric materials. Int. J. Solids Struct. 37, 3210–3229.

Erdogan, F., Gupta, G.D., 1972. On the numerical solution of singular integral equation. Quart. J. Mech. Appl. Math. 29, 525–534.

Fan, H., Sze, K.Y., Yang, W., 1996. Two-dimensional contact on a piezoelectric half-space. Int. J. Solids Struct. 33, 1305–1315.

Galassi, C., Dinescu, M., Uchino, K., Sayer, M. (Eds.), 2000. Piezoelectric Materials: Advances in Science, Technology and Applications. Kluwer, Netherlands.

Giannakopoulos, A.E., Suresh, S., 1999. Theory of indentation of piezoelectric materials. Acta Mater. 47, 2153–2164.

Irschik, H., Ziegler, E., 1996. Maysel's formula generalized for piezoelectric vibrations: application to thin shells of revolution. AIAA J. 34, 2402–2405.

Ke, L.L., Yang, J., Kitipornchai, S., Wang, Y.S., 2008. Electro-mechanical frictionless contact behavior of a functionally graded piezoelectric layered half-plane under a rigid punch. Int. J. Solids Struct. 45, 3313–3333.

Ke, L.L., Wang, Y.S., Yang, J., Kitipornchai, S., 2010. Sliding frictional contact analysis of functionally graded piezoelectric layered half-plane. Acta. Mech. 209, 249–268.

Ootao, Y., 2009. Transient thermoelastic and piezothermoelastic problems of functionally graded materials. J. Thermal Stress. 32, 656–697.

Ootao, Y., Tanigawa, Y., 2001. Control of the transient thermoelastic displacement of a functionally graded rectangular plate bonded to a piezoelectric plate due to nonuniform heating. Acta Mech. 148, 17–33.

Ootao, Y., Tanigawa, Y., 2007. Transient piezothermoelastic analysis for a functionally graded thermopiezoelectric hollow sphere. Compos. Struct. 81, 540–549.

Ootao, Y., Akai, T., Tanigawa, Y., 2008. Transient piezothermoelastic analysis for a functionally graded thermopiezoelectric hollow cylinder. J. Thermal Stress. 31, 935–955.

Podilchuk, Y.N., Tkachenko, V.F., 1999. The contact problem of electroelasticity for a flat punch with parabolic cross-section. Int. Appl. Mech. 35, 1096–1103.

Ramamurty, U., Sridhar, S., Giannakopoulos, A.E., Suresh, S., 1999. An experimental study of spherical indentation on piezoelectric materials. Acta Mater. 47, 2417–2430.

Saigal, A., Giannakopoulos, A.E., Pettermann, H.E., Suresh, S., 1999. Electric response during indentation of a piezoelectric ceramic–polymer composite. J. Appl. Phys. 86, 603–606.

Sosa, H.A., Castro, M.A., 1994. On concentrated loads at the boundary of a piezoelectric half-plane. J. Mech. Phys. Solids 42, 1105–1122.

Sridhar, S., Giannakopoulos, A.E., Suresh, S., 2000. Mechanical and electrical response of piezoelectric solids to conical indentation. J. Appl. Phys. 87, 8451–8456.

Tauchert, T.R., Ashida, F., Noda, N., Adali, S., Verijenko, V., 2000. Developments in thermopiezoelasticity with relevance to smart composite structures. Compos. Struct. 48, 31–38.

Wang, B.L., Han, J.C., 2006. A circular indenter on a piezoelectric layer. Arch. Appl. Mech. 76, 367–379.

Wang, B.L., Noda, N., 2001. Design of a smart functionally graded thermopiezoelectric composite structure. Smart Mater. Struct. 10, 189–193.

Wang, B.L., Han, J.C., Du, S.Y., Zhang, H.Y., Sun, Y.G., 2008. Electromechanical behavior of a finite piezoelectric layer under a flat punch. Int. J. Solids Struct. 45, 6384–6398.

Weeks, W.T., 1966. Numerical inversion of the laplace transforms using Lagurre functions. J. Assoc. Comput. Mach. 13, 419–429.

Wu, X.H., Shen, Y.P., Chen, C., 2003. An exact solution for functionally graded piezothermoelastic cylindrical shell as sensors or actuator. Mater. Lett. 57, 3532–3542.

Zhong, Z., Shang, E., 2005. Exact analysis of simply supported functionally graded piezothermoelectric plates. J. Intell. Mater. Syst. Struct. 16, 643–651.